Supplement of Atmos. Chem. Phys., 25, 2087–2121, 2025
https://doi.org/10.5194/acp-25-2087-2025-supplement

Atmospheric Chemistry and Physics
Open Access
EGU

Supplement of

Tropospheric aerosols over the western North Atlantic Ocean during the winter and summer deployments of ACTIVATE 2020: life cycle, transport, and distribution

Hongyu Liu et al.

Correspondence to: Hongyu Liu (hongyu.liu-1@nasa.gov) and Bo Zhang (bo.zhang@nasa.gov)

Section S1: Anthropogenic, biogenic, marine DMS, and lightning NO_x emissions in GEOS-Chem

Global anthropogenic emissions are based on the EDGAR v4.2 emissions inventory for 2008. We use the 2011 EPA National Emissions Inventory (NEI11) emissions as implemented by Travis et al. (2016) over the U.S. with national annual scaling factor updated for 2018 (Yu et al., 2018), CAC emissions inventory over Canada, BRAVO emissions inventory over Mexico, EMEP emissions inventory over Europe, and the MIX emissions inventory (for year 2010) over China (Li et al., 2014). Shipping emissions are from the EMEP inventory (Vestreng et al., 2007). Aircraft emissions are from the AEIC inventory for 2005 (Stettler et al., 2011). The NEI11 emissions inventory contains biofuel emissions. Biogenic emissions are calculated online using the MEGAN model (Guenther et al., 2012). Marine DMS emissions are calculated as a product of the climatological monthly mean surface seawater DMS concentration (Lana et al., 2011) and sea-to-air transfer velocity, as implemented by Breider et al. (2017). Lightning NO_x emissions are constrained by the Lightning Imaging Sensor and the Optical Transient Detector (LIS/OTD) climatological observations of lightning flashes, as described by Murray et al. (2012).

Section S2: Surface aerosol observations, MODIS AOD, and CALIPSO data quality screening

CSN, IMPROVE, and NADP. Surface aerosol composition (SO_4^{2-}, NO_3^-, NH_4^+) data for the eastern U.S. were obtained from the Chemical Speciation Network (CSN) and the Interagency Monitoring of Protected Visual Environments (IMPROVE) network (Solomon et al., 2014; Malm et al., 1994). IMROVE does not include NH_4^+ measurements. Daily observational data for 2020 were obtained from the Federal Land Manager Environmental Database at the Cooperative Institute for Research in the Atmosphere (CIRA), Colorado State University (https://views.cira.colostate.edu/fed; last access on 31 July 2022). The readers are referred to that website for methods of chemical characterization, uncertainties, detection limits, and data downloading. Aerosol wet deposition composition (SO_4^{2-}, NO_3^-, NH_4^+) data from the ensemble of eastern U.S. sites are from the National Trends Network (NTN) of the U.S. National Atmospheric Deposition Program (NADP, https://nadp.slh.wisc.edu/). The NTN measures total weekly wet deposition of SO_4^{2-}, NH_4^+, and NO_3^- and we use monthly mean data downloaded from http://views.cira.colostate.edu/fed/. Since the NTN wet deposition of SO_4^{2-} includes contribution from SO_4^{2-} resulting from oxidation of SO_2 in rainwater, for comparison with NTN measurements we calculate the model sulfur wet deposition fluxes as the sum of the SO_4^{2-} wet deposition flux and 150% (based on the ratio of the molar masses of SO_2 and SO_4^{2-}) of the model estimated SO_2 wet deposition (Appel et al., 2011). Similarly, the model estimates of NO_3^- (NH_4^+) wet deposition include 98.4% (106%) of the model estimates of HNO_3 (NH_3) wet deposition. Gartman (2017) described the analysis and quality assurance of the NADP data. The IMPROVE and NADP data sets were previously used by Corral et al. (2020, 2021) to analyze aerosols and wet deposition chemistry over the U.S. East Coast.

MODIS. Satellite retrieved products of AODs are available from the Moderate Resolution Imaging Spectroradiometer (MODIS) on Aqua. MODIS has a ~2330 km swath and provides nearly global coverage daily. We use the MODIS/Aqua Level 3 daily (MYD08_D3) AOD product at 550 nm and 1°×1° horizontal resolution (Collection 6.1; scientific data set or SDS named "Aerosol_Optical_Depth_Land_Ocean_Mean") from the Dark Target (DT) retrieval algorithm (Sayer et al., 2014; Levy et al., 2013; Hubanks et al., 2019). This SDS contains only AOD values for any DT-ocean retrieval having the Quality Assurance Confidence (QAC) >=1 and any DT-land retrievals having

QAC=2 (good confidence) or 3 (high confidence) (Levy et al., 2013; R.C. Levy, personal communication, 2019). Collection 6.1 data are available from https://ladsweb.modaps.eosdis.nasa.gov/search/.

CALIPSO. The data averaging approach used to generate the CALIPSO version 4 Level 3 aerosol products are used in this study (Tackett et al., 2018). The following quality screening and data selection techniques are applied:

1) When creating the averaged profiles used in this work, CALIOP Level 2 range bins in "clear air" regions where no aerosol is detected are typically assigned aerosol extinction coefficients of 0 km^{-1}. An exception to this convention is exercised for regions of "clear air" lying below aerosol layers with base heights lower than 250 m. Because we assume the atmosphere is well mixed below 250 m, excluding these bins avoids introducing low biases near the Earth's surface.

2) Aerosol layers detected at 80 km horizontal resolution that are not vertically or horizontally adjacent to another aerosol layer detected at finer spatial resolutions (i.e., 5 km or 20 km) are assumed to be noise-induced false positive detections, and hence are discarded.

3) Layers classified as aerosols that are detected at 80 km horizontal resolution with base altitudes above 4 km and are in contact with ice clouds are assumed to be misclassified cirrus "fringes" (Liu et al., 2019), and are also discarded.

4) Aerosol samples in the surface-attached opaque layer (beneath the maximum surface elevation), for which the extinction is greater than 2 km^{-1} and at least 10 times higher than the extinction of the layer above, are rejected to avoid surface contamination.

5) In any 5-km profile in the CALIOP Level 2 data product, range bins identified as aerosol that have embedded cloud fractions greater than 97% are rejected, as are all samples at lower altitudes in the profile. Rejecting these samples reduces the likelihood of cloud contamination.

The details of the quality screening to generate the Level 3 aerosol profile product are described in Winker et al. (2013), Tackett et al. (2018), and the CALIPSO Data Users' Guide (https://www-calipso.larc.nasa.gov/resources/calipso_users_guide/).

Section S3: Model evaluation with surface aerosol concentrations, deposition fluxes, and MODIS AOD observations

In this section we evaluate model simulations with surface aerosol concentration observations from the IMPROVE and CSN networks, aerosol deposition flux measurements from the NTN network of NADP, and satellite AOD measurements from MODIS/Aqua, with a focus on the eastern U.S. coastal region or WNAO.

Aerosol surface concentrations. For comparison with model SNA surface concentrations, we use the IMPROVE/CSN observations obtained at 59 eastern U.S. sites (in the states of NY, CT, VA, MA, ME, GA, PA, DC, FL, NC, and SC), which are located upwind of the ACTIVATE flight area. **Fig. S1** shows the scatterplots of IMPROVE/CSN daily surface concentrations of SNA aerosols versus corresponding model results at each of the selected sites for Feb.-Mar. (upper panels) and Aug.-Sep. (lower panels), respectively, 2020. The model results from both "standard" (blue triangles and lines) and "fixedCWC" (red triangles and lines) experiments (also see **Table 1**) are shown to help understand the impact of using MERRA-2 CWC on simulated aerosols in GEOS-Chem. Model

daily output was sampled at the day, location, and site elevation for each data sample. In Feb.-Mar., for sulfate the standard model with MERRA-2 CWC has a small overall bias (0.6%) relative to the observations, with a reduced-major-axis (RMA) regression slope of 0.80 and a correlation coefficient (R) value of 0.46. The fixedCWC simulation yields a better regression slope (0.98) but a much larger overall bias. The standard model overestimates nitrate and ammonium substantially with an average positive bias of 198.5% and 230.3%, respectively. These biases in fixedCWC are even higher. Using MERRA-2 CWC in the stratiform precipitation scavenging in the standard model is expected to reduce existing large positive biases in surface nitrate and ammonium concentrations as demonstrated by Luo et al. (2019, 2020). Our results here also show that using spatiotemporally varying CWC from MERRA-2 slightly expedites aerosol scavenging and thus improves simulated aerosol concentrations. The improvement in our analysis is, however, very limited. In Aug.-Sep., the standard model largely overestimates surface concentrations of sulfate (61.2% bias), nitrate (97.4% bias), and ammonium (249.9% bias). Using MERRA-2 CWC has slightly reduced the model bias in surface sulfate concentrations but increased the model biases in surface nitrate and ammonium concentrations. The latter is inconsistent with Luo et al. (2020) probably due to not having fully implemented their modifications to sulfate scavenging, which affects nitrate and ammonium through the SNA aerosol chemical dynamics. This also suggests that the impact of individual modifications to SNA wet scavenging should be investigated separately because feedback from complicated chemical dynamics is always involved.

Aerosol wet deposition fluxes. For comparison with model SNA wet deposition fluxes, we use the NADP observations obtained at over 100 eastern U.S. sites (in the same states as for surface aerosol concentrations above). **Fig. S2** shows the scatterplots of model monthly mean wet deposition fluxes of sulfate + SO_2, nitrate + nitric acid (HNO_3), and ammonium + ammonia (NH_3) versus those from NADP for Feb.-Mar. and Aug.-Sep. 2020. The observed sulfur deposition fluxes are mostly < 1.0 kg per ha per 30 days and did not change significantly from winter to summer. In both seasons, the standard model with MERRA-2 CWC overestimates sulfate wet deposition fluxes (~57.9% bias in winter and ~44.2% bias in summer), while the fixedCWC simulation results in reduced biases (~18.4% in winter and 31.8% in summer). Correlation between either of the two simulations and observations is not strong ($R<0.5$), suggesting that further improvement is required for sulfate scavenging. Observed wet deposition fluxes of nitrate tend to decrease from winter to summer, presumably because of lower concentrations in summer (**Fig. S1**). In the wintertime, both the standard and fixedCWC simulations overestimate nitrate deposition fluxes. The fact that model simulations show large positive biases in both surface concentrations and deposition fluxes suggests that there is too much nitrate mass in the model and/or nitrate is scavenged too fast at higher altitudes followed by partial release into the air due to rainwater evaporation close to the surface. Compared to the fixedCWC simulation, the standard simulation shows larger nitrate deposition flux overestimates due to faster scavenging with MERRA-2 CWC (Luo et al., 2019). The observed ammonium wet deposition fluxes exhibit larger variability among all sites in summer relative to winter. The fixedCWC simulation tends to underestimate ammonium deposition fluxes and shows values of similar magnitude in the two seasons. The standard simulation with MERRA-2 CWC overcorrects this underestimate in winter due to enhanced stratiform precipitation scavenging of ammonium, resulting in an overall positive bias of 46.1%. Such effects are not seen for summertime ammonium likely because of the increased role of convective scavenging in summer.

MODIS AOD. We compare model simulated AOD with MODIS observations with respect to the spatial distribution of monthly mean AODs along with speciated AODs suggested by the model. **Fig. S3** shows model monthly mean AODs in comparison with MODIS/Aqua retrievals (at 550 nm) over North America and the North Atlantic for the months of Feb. and Mar., respectively, 2020. Model output is sampled daily at ~1:30 pm local time along the Aqua satellite orbit track. Also shown are contributions to the total AOD in the model from accumulation mode sea salt (SSa), coarse mode sea salt (SSc), SNA, BC, organic carbon (OC), and dust. Model AODs in the simulation "fixedCWC" (**Table 1**) are shown in the bottom panels. In general, the model underestimates AODs over the WNAO during Feb.-Mar. 2020, with improved model performances along the south/east U.S. coast in March. The former is likely ascribed to underestimated sea salt emissions because of MERRA-2's tendency to underestimate ocean surface winds (Carvalho, 2019) and coarse model grid resolution (Weng et al., 2020). The spatial variation of MODIS AOD from the Midwest U.S. to the WNAO shows different patterns between Feb. and Mar. In Feb., MODIS observed high AODs over the Midwest U.S., a decreasing trend towards the South/East U.S. Coast, and high AODs over the WNAO. The model captures this spatial pattern but the magnitude of AOD variations is much smaller than observed by MODIS. The spatial distribution of model simulated speciated AODs (**Fig. S3**) suggest that SNA aerosols over the Midwest U.S. and coarse-mode sea salt over the WNAO are mainly responsible for this pattern in Feb. In Mar., MODIS observed higher AODs in South/East U.S. Coast and over the WNAO compared to Feb. Such increases are also captured by the model, which attributes the higher AODs to substantially increased OC and, to a lesser extent, more SNA over the Midwest U.S. and coarse-mode sea salt over the WNAO. The low bias in AOD over the western U.S. in the model is likely due to missing anthropogenic or BB emissions for the region, as the "fixedCWC" simulation with slower wet scavenging does not remove this model bias. The latter simulation does yield higher AODs over the WNAO, closer to the MODIS values. However, this could be a result of compensating effects between inefficient aerosol wet scavenging and low sea salt emissions over the ocean. Model simulated AODs over the WNAO are dominated by coarse-mode sea salt, SNA, OC, and accumulation-mode sea salt, with negligible contributions from BC and dust.

Fig. S4 shows the same plots as **Fig. S3**, but for the months of Aug. and Sep., respectively, 2020. In Aug., MODIS observed much higher AODs over the western, southwestern, southeastern U.S., and WNAO, relative to the winter months. The model reproduces the general spatial distribution but again underestimates AODs over the remote Atlantic Ocean. The distribution of model speciated AODs suggests that OC explains most of the AOD spatial variation while SNA also makes an important contribution. In September, MODIS observed even higher AODs over the western U.S. coast (> 0.5), Midwest U.S., and WNAO. The model captures this month-to-month change in AODs very well and attributes it to large increases in OC as well as coarse-mode sea salt aerosols. As expected, SNA AOD decreases from Aug. to Sep., reflecting the seasonal reduction in secondary production of SNA aerosols. In summer 2020, extensive wildfires occurred in the western and southeastern U.S. (section 4.4). In particular, the August Complex "Gigafire" in mid-August 2020 and the California Creek fire in early September 2020 are among the most intensive fire events in California. Primary organic aerosols and SOA from oxidation of VOCs emitted by these fires cause substantial increases in AOD over both the fire emission source region and along the smoke transport pathway towards the Midwest, northeast U.S., and WNAO, as observed by MODIS and simulated by the model. The generally much higher

AODs in summer relative to winter are mainly due to the much larger contributions from these smoke organic aerosols. The model AOD low bias over the WNAO in Aug. appears to be at least partly due to underestimate of sea salt emissions, which are lower than those for Feb., Mar., and Sep. In addition, BC from the wildfires makes non-negligible contributions to summertime AOD over the western and Midwest U.S., in contrast to the wintertime. Model dust AOD distributions indicate transport of dust from tropical eastern Atlantic and North Africa to the WNAO region during the summer months, especially Aug. 2020, in agreement with MODIS AOD observations. Using MERRA-2 CWC for stratiform precipitation scavenging of aerosol in the standard model has little effects on model simulated AOD in Aug.-Sep., when compared to those from the "fixedCWC" simulation (bottom panels, **Fig. S4**). This is due to the dominant role of convective (versus stratiform) precipitation in scavenging aerosols during summer.

References

Appel, K. W., Foley, K. M., Bash, J. O., Pinder, R. W., Dennis, R. L., Allen, D. J., and Pickering, K.: A multi-resolution assessment of the Community Multiscale Air Quality (CMAQ) model v4.7 wet deposition estimates for 2002–2006, Geosci. Model Dev., 4, 357–371, https://doi.org/10.5194/gmd-4-357-2011, 2011.

Breider, T.J., L.J. Mickley, D.J. Jacob, C. Ge, J. Wang, M.P. Sulprizio, B. Croft, D.A. Ridley, J.R. McConnell, S. Sharma, L. Husain, V.A. Dutkiewicz, K. Eleftheriadis, H. Skov, and P.K. Hopke, Multi-decadal trends in aerosol radiative forcing over the Arctic: contribution of changes in anthropogenic aerosol to Arctic warming since 1980, J. Geophys. Res., 122(6), 3573â€“3594, doi:10.1002/2016JD025321, 2017.

Carvalho, D.: An Assessment of NASA's GMAO MERRA-2 Reanalysis Surface Winds, J. Climate, 32(23), 8261–8281, doi:10.1175/JCLI-D-19-0199.1, 2019.

Corral, A. F., Dadashazar, H., Stahl, C., Edwards, E.-L., Zuidema, P., and Sorooshian, A.: Source Apportionment of Aerosol at a Coastal Site and Relationships with Precipitation Chemistry: A Case Study over the Southeast United States, Atmosphere, 11, 1212, https://doi.org/10.3390/atmos11111212, 2020.

Corral, A. F., Braun, R. A., Cairns, B., Gorooh, V. A., Liu, H., Ma, L., et al.: An overview of atmospheric features over the Western North Atlantic Ocean and North American East Coast – Part 1: Analysis of aerosols, gases, and wet deposition chemistry. Journal of Geophysical Research: Atmospheres, 126, e2020JD032592. https://doi.org/10.1029/2020JD032592, 2021.Gartman, N.: Quality Assurance Report National Atmospheric Deposition Program 2016, https://nadp.slh.wisc.edu/wp-content/uploads/2021/04/cal_qar_2016.pdf, 2017.

Guenther, A. B., Jiang, X., Heald, C. L., Sakulyanontvittaya, T., Duhl, T., Emmons, L. K., and Wang, X.: The Model of Emissions of Gases and Aerosols from Nature version 2.1 (MEGAN2.1): an extended and updated framework for modeling biogenic emissions, Geosci. Model Dev., 5, 1471-1492, https://doi.org/10.5194/gmd-5-1471-2012, 2012.

Lana, A., et al.: An updated climatology of surface dimethlysulfide concentrations and emission fluxes in the global ocean, Global Biogeochem. Cycles, 25, GB1004, doi:10.1029/2010GB003850, 2011.

Li, M., Zhang, Q., Streets, D. G., He, K. B., Cheng, Y. F., Emmons, L. K., et al.: Mapping Asian anthropogenic emissions of non-methane volatile organic compounds to multiple chemical mechanisms. Atmospheric Chemistry and Physics, 14, 5617–5638. https://doi.org/10.5194/acp-14-5617-2014, 2014.

Liu, Z., J. Kar, S. Zeng, J. Tackett, M. Vaughan, M. Avery, J. Pelon, B. Getzewich, K.-P. Lee, B. Magill, A. Omar, P. Lucker, C. Trepte, and D. Winker: Discriminating Between Clouds and Aerosols in the CALIOP Version 4.1 Data Products, *Atmos. Meas. Tech.*, **12**, 703–734, https://doi.org/10.5194/amt-12-703-2019, 2019.

Murray, L. T., Jacob, D. J., Logan, J. A., Hudman, R. C., and Koshak, W. J.: Optimized regional and interannual variability of lightning in a global chemical transport model constrained by LIS/OTD satellite data, J. Geophys. Res., 117, D20307, doi:10.1029/2012JD017934, 2012.

Philip, S, Marin, R. V., Pierce, J. R., Jimenez, J. L., Zhang, Q., Canagaratna, M. R., Spracklen, D. V., Nowlan, C. R., Lamsal, L. N., Cooper, M. J., and Krotkov, N. A., Spatially and seasonally resolved estimate of the ratio of organic mass to organic carbon, Atmos. Environ., 87, 34-40, http://dx.doi.org/10.1016/j.atmosenv.2013.11.065, 2014.

Stettler, M. E. J., Eastham, S., Barrett, S. R. H.: Air quality and public health impacts of UK airports. Part I: Emissions. Atmospheric Environment, 45(31), 5415–5424. https://doi.org/10.1016/j.atmosenv.2011.07.012, 2011.

Tackett, J. L., Winker, D. M., Getzewich, B. J., Vaughan, M. A., Young, S. A., and Kar, J.: CALIPSO lidar level 3 aerosol profile product: Version 3 algorithm design. Atmospheric Measurement Techniques, 11(7), 4129–4152. https://doi.org/10.5194/amt-11-4129-2018, 2018.

Travis, K. R., Jacob, D. J., Fisher, J. A., Kim, P. S., Marais, E. A., Zhu, L., et al.: Why do models overestimate surface ozone in the Southeast United States? Atmos. Chem. Phys., 16, 13,561–13,577. https://doi.org/10.5194/acp-16-13561-2016, 2016.

Vestreng, V., Mareckova, K., Kakareka, S., Malchykhina, A., and Kukharchyk, T., Inventory Review 2007; Emission Data Reported to LRTAP Convention and NEC Directive, MSC-W Technical Report 1/07, The Norwegian Meteorological Institute, Oslo, Norway, 2007. https://emep.int/publ/reports/2007/emep_technical_1_2007.pdf

Weng, H.-J., Lin, J.-T. *, Martin, R., Millet, D. B., Jaeglé, L., Ridley, D., Keller, C., Li, C., Du, M.-X., and Meng, J., Global high-resolution emissions of soil NOx, sea salt aerosols, and biogenic volatile organic compounds, Scientific Data, 7, 148, doi:10.1038/s41597-020-0488-5, 2020.

Winker, D. M., Tackett, J. L., Getzewich, B. J., Liu, Z., Vaughan, M. A., and Rogers, R. R.: The global 3-D distribution of tropospheric aerosols as characterized by CALIOP, Atmos. Chem. Phys., 13, 3345–3361, https://doi.org/10.5194/acp-13-3345-2013, 2013.Yu, F., A. Nair, and G. Luo: Long term trend of gaseous ammonia in US: Modeling and comparison with observations, Journal of Geophysical Research: Atmospheres, 123, 8315-8325, 2018.

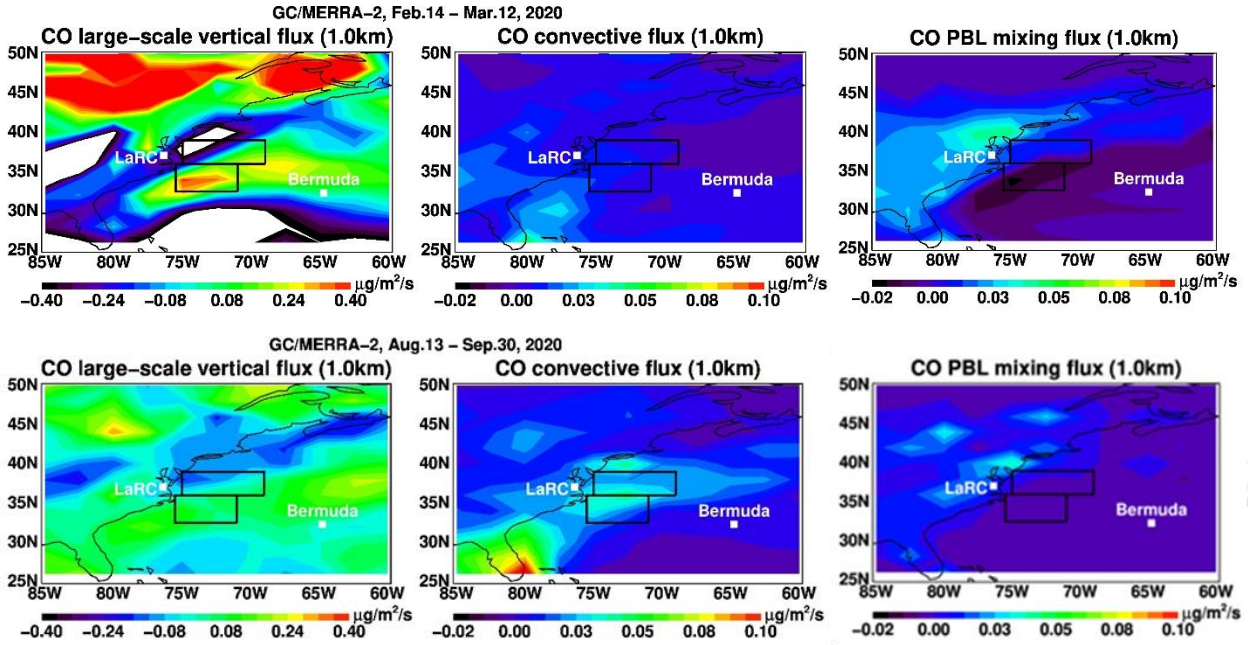

Figure S1a. Model simulated large-scale (resolved) vertical fluxes, convective fluxes, and PBL turbulent mixing fluxes of CO at the altitude of 1.0 km, averaged over the periods of Feb. 14 - Mar. 12 (upper row) and Aug. 13 – Sep. 30 (lower row), 2020, respectively. White areas indicate saturated values. The two rectangular boxes denote major flight areas (see "N" and "S" in Fig. 1).

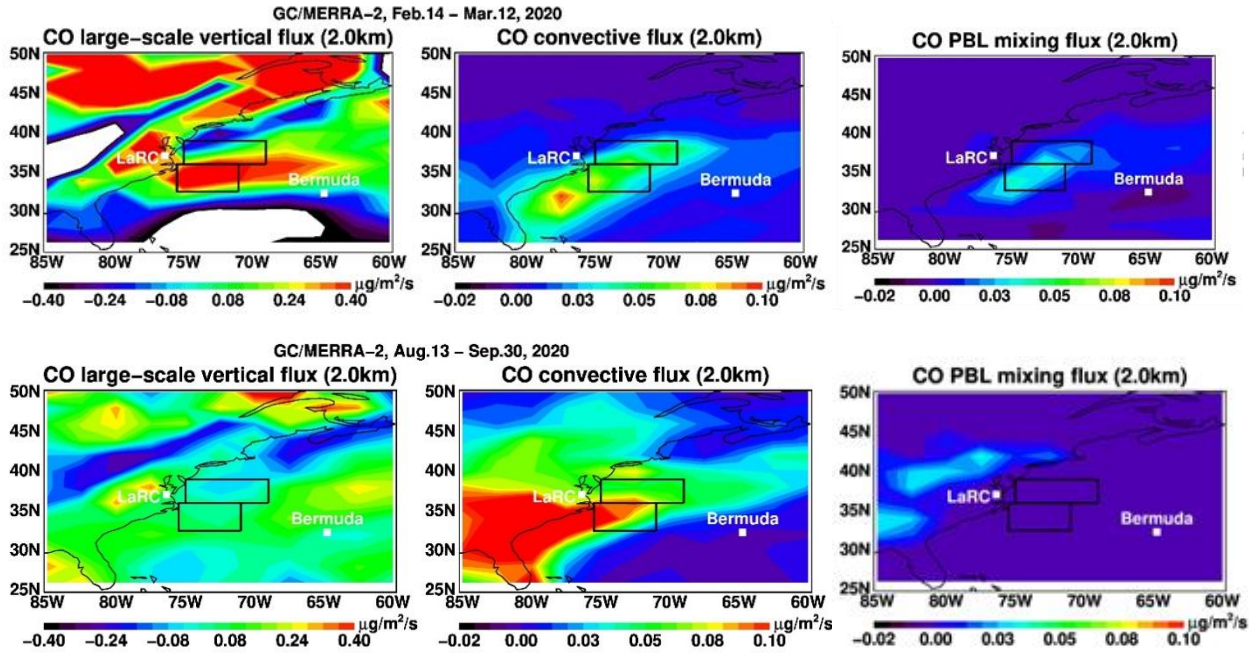

Figure S1b. Same as Fig. S1a, but for the altitude of 2.0 km. White areas indicate saturated values.

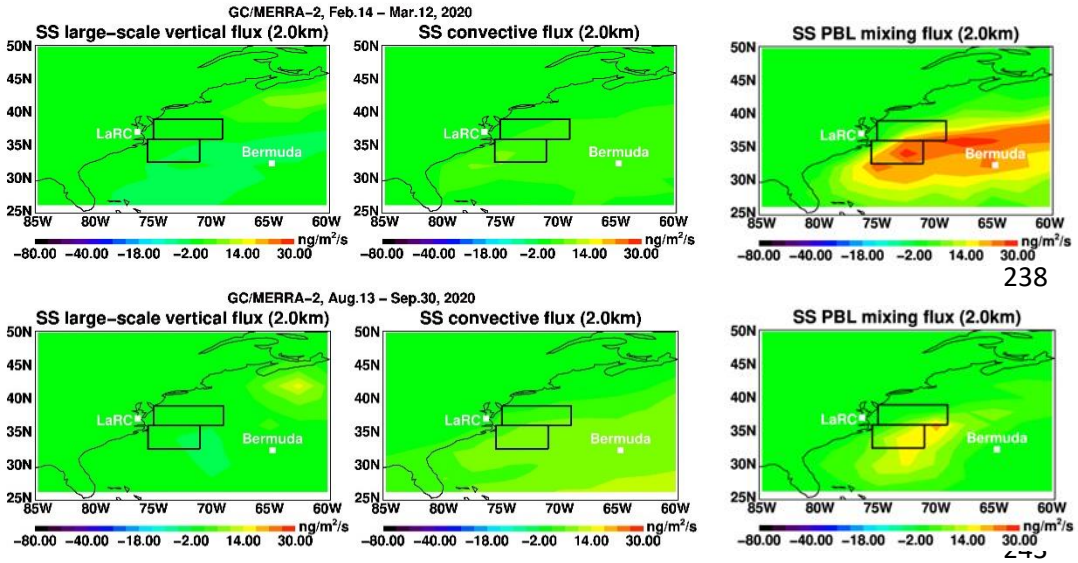

Figure S1c. Same as Fig. S1a, but for sea salt at the altitude of 2.0 km.

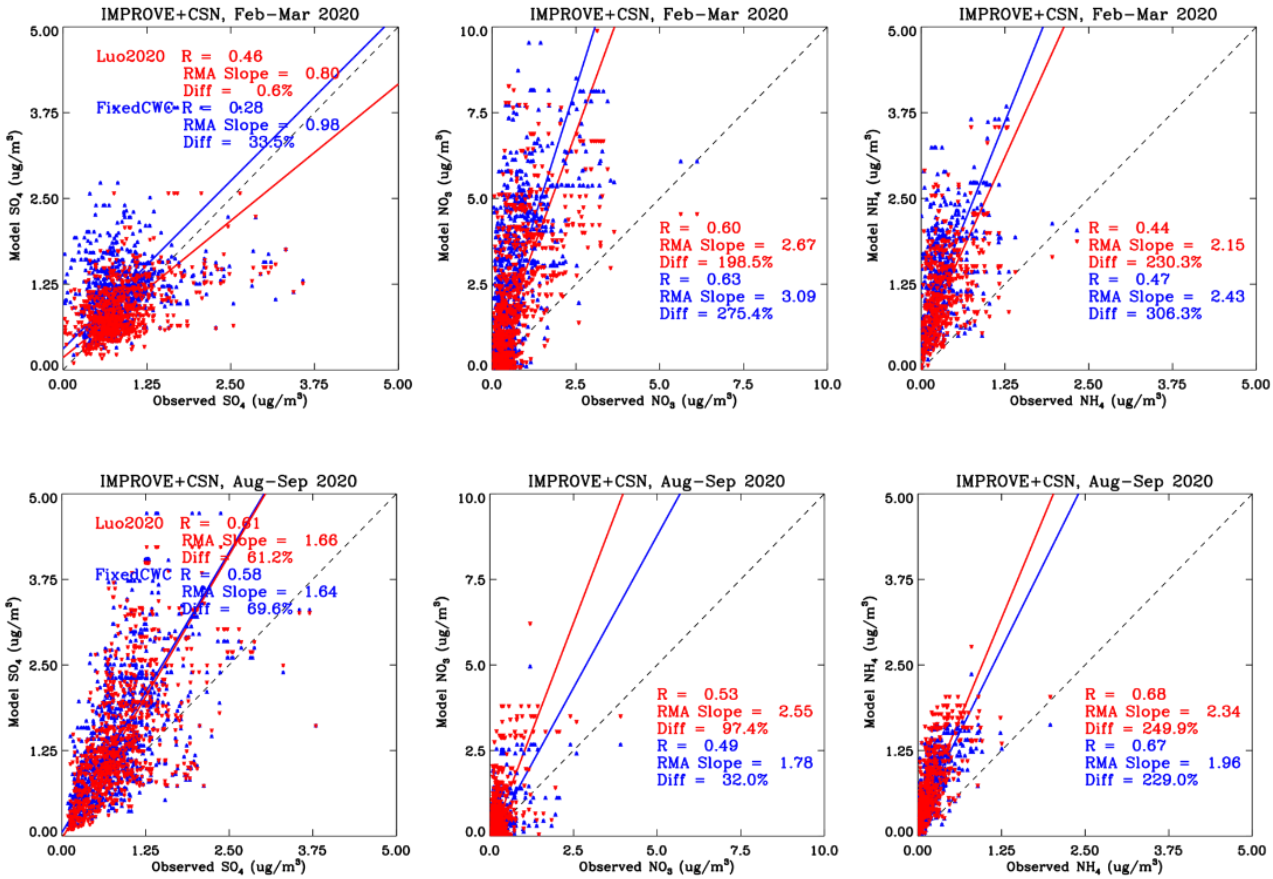

Figure S2. Scatterplots of model daily mean surface concentrations of SO_4, NO_3, and NH_4 versus corresponding IMPROVE and CSN observations made at near-coast eastern U.S. sites during Feb.-Mar. (upper panels) and Aug.-Sep. (lower panels) 2020, respectively. Model results from simulations with either a fixed cloud water content (blue; Table 1) or MERRA-2 cloud water content (red; Table 1) are shown. Solid lines are the linear regression lines obtained using the reduced-major-axis (RMA) method. Dashed lines are 1:1 line. Legends show calculated correlation coefficient, RMA slope (if R > 0.1), and overall difference (%) between model results and observations, i.e., ($\Sigma model$ - $\Sigma observation$) / $\Sigma observation$ × 100%.

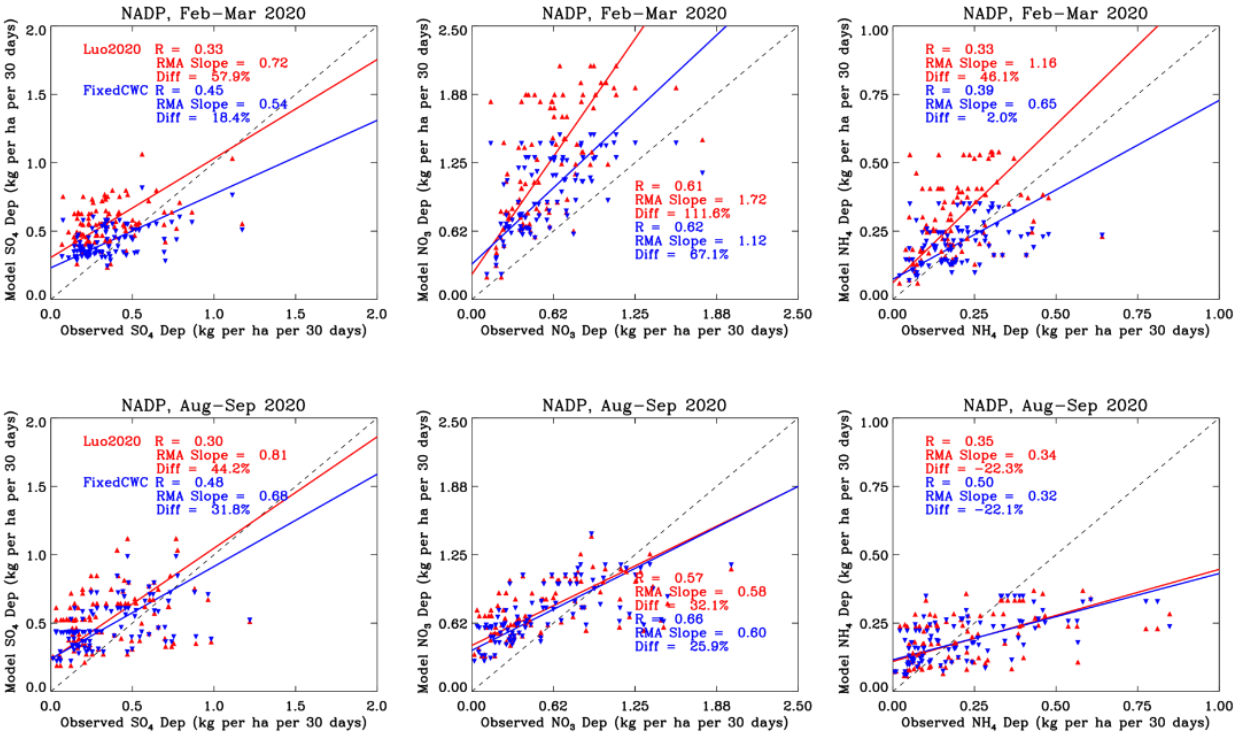

Figure S3. Scatterplots of model monthly mean wet deposition fluxes of SO_4+SO_2, NO_3+HNO_3, and NH_4+NH_3 versus corresponding NADP observations made at near-coast eastern U.S. sites (>100 sites in the states of NY, CT, VA, MA, ME, GA, PA, DC, FL, NC, and SC) during Feb.-Mar. (upper panels) and Aug.-Sep. (lower panels) 2020, respectively. Deposition mass fluxes of SO_2, HNO_3, and NH_3 are converted to SO_4, NO_3, and NH_3 mass fluxes of equivalent mole amounts. Monthly mean model results are sampled at the month and location of observations. Each data point in the figure represents a monthly mean value for one single site. Model results from simulations with either a fixed cloud water content (blue; Table 1) or MERRA-2 cloud water content (red; Table 1) are shown. Solid lines are the linear regression lines obtained using the reduced-major-axis (RMA) method. Dashed lines are 1:1 line. Legends show calculated correlation coefficient), RMA slope (if R > 0.1), and overall difference (%) between model results and observations: (Σ*model* - Σ*observation*) / Σ*observation* × 100%.

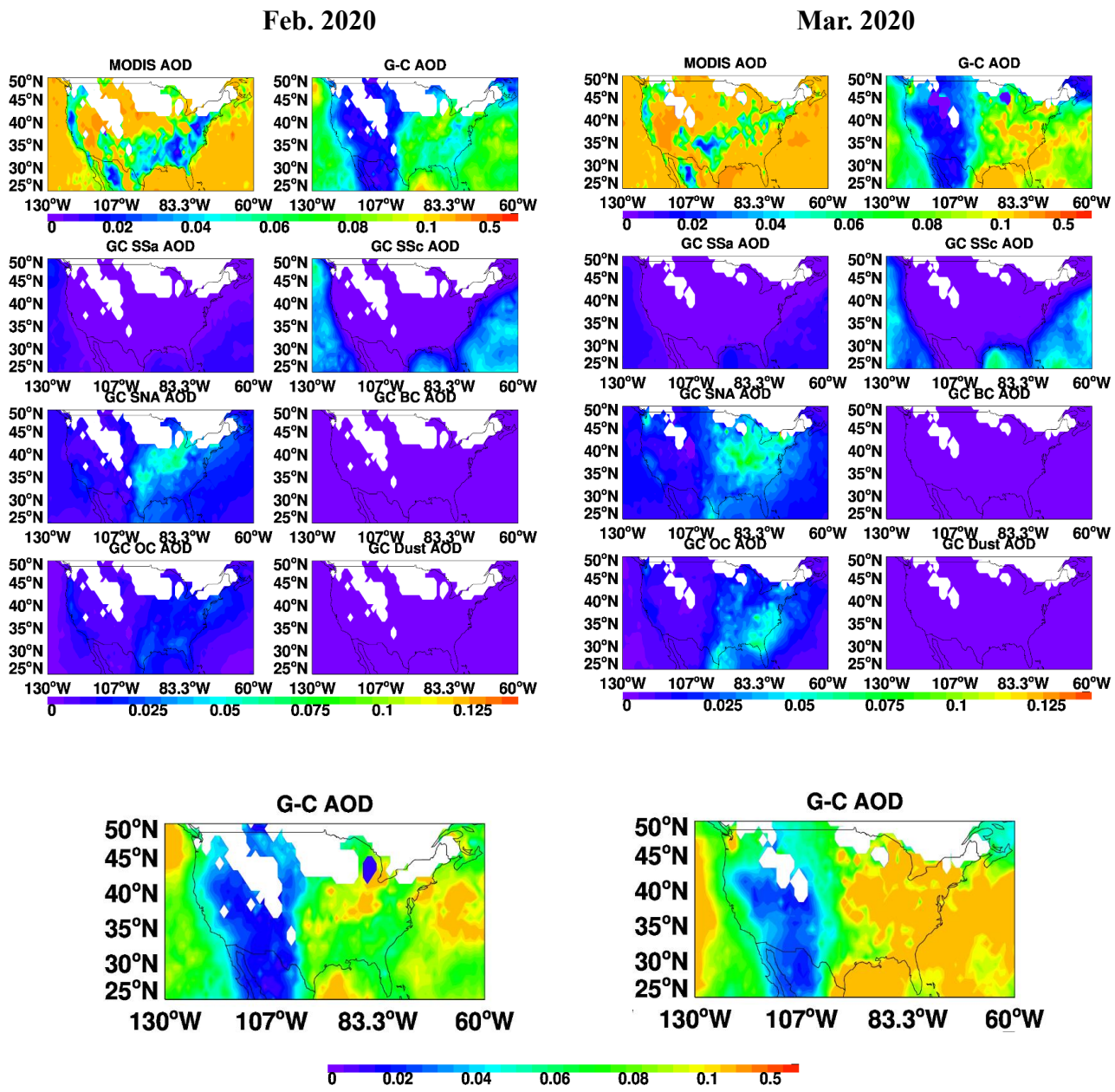

Figure S4. Evaluation of model monthly mean AODs with MODIS/Aqua retrievals (at 550nm) over North America and North Atlantic for Feb. 2020 (left two columns) and Mar. 2020 (right two columns). Model output is sampled daily at 1:30 pm local time along the Aqua satellite orbit track. Also shown are contributions to the total AOD in the model from accumulation mode sea salt (SSa), coarse mode sea salt (SSc), sulfate-nitrate-ammonium (SNA), black carbon (BC), organic carbon (OC, primary only), and dust. Model AODs in the simulation "fixedCWC" (Table 1) are shown in the bottom panels.

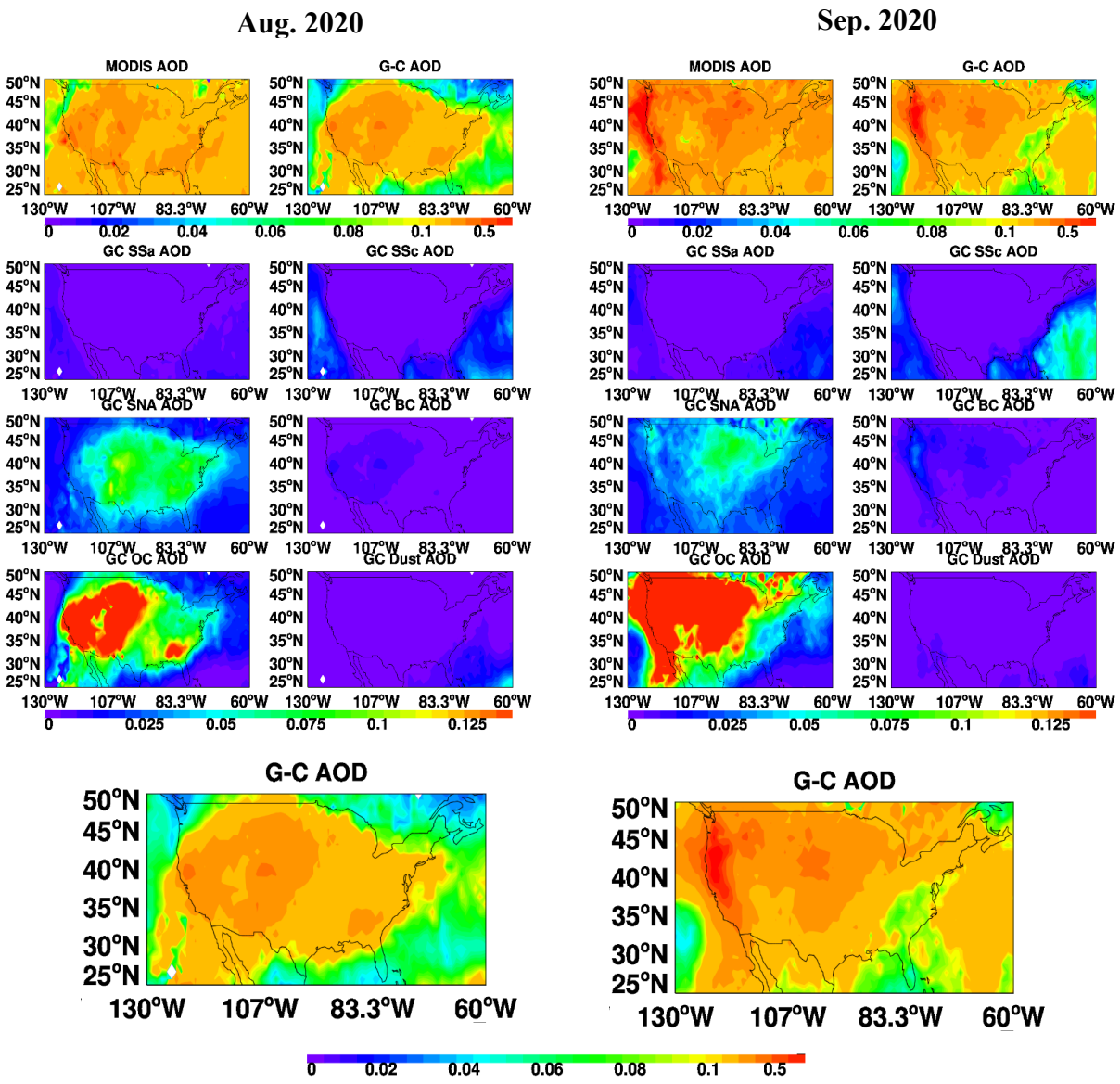

Figure S5. Same as Fig. S4, but for Aug. 2020 (left two columns) and Sep. 2020 (right two columns).

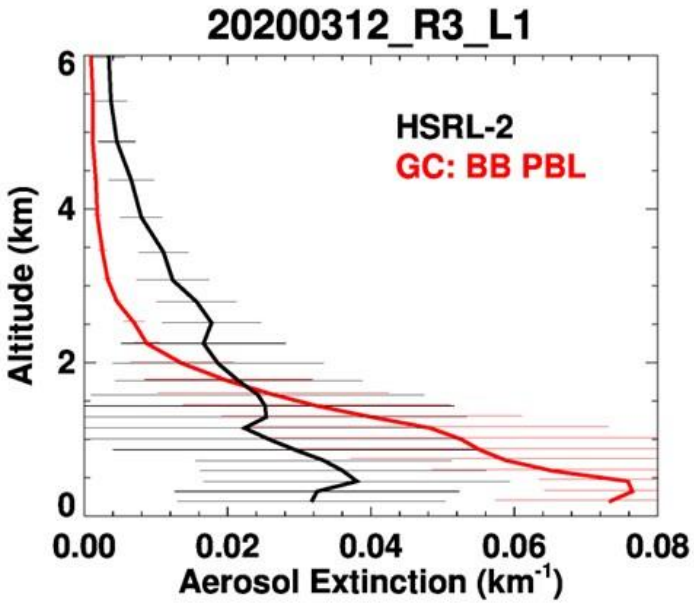

Figure S6. Comparisons of model aerosol extinctions (550nm) with aircraft HSRL-2 lidar measurements (532nm) averaged over the morning flight on March 12, 2020. Biomass burning emissions are injected into the planetary boundary layer ("BB PBL") in the model (see Table 1). Hourly model output was sampled at the time and location of lidar measurements. Horizontal lines denote +/- standard deviations of observed and simulated aerosol extinctions at model vertical levels.

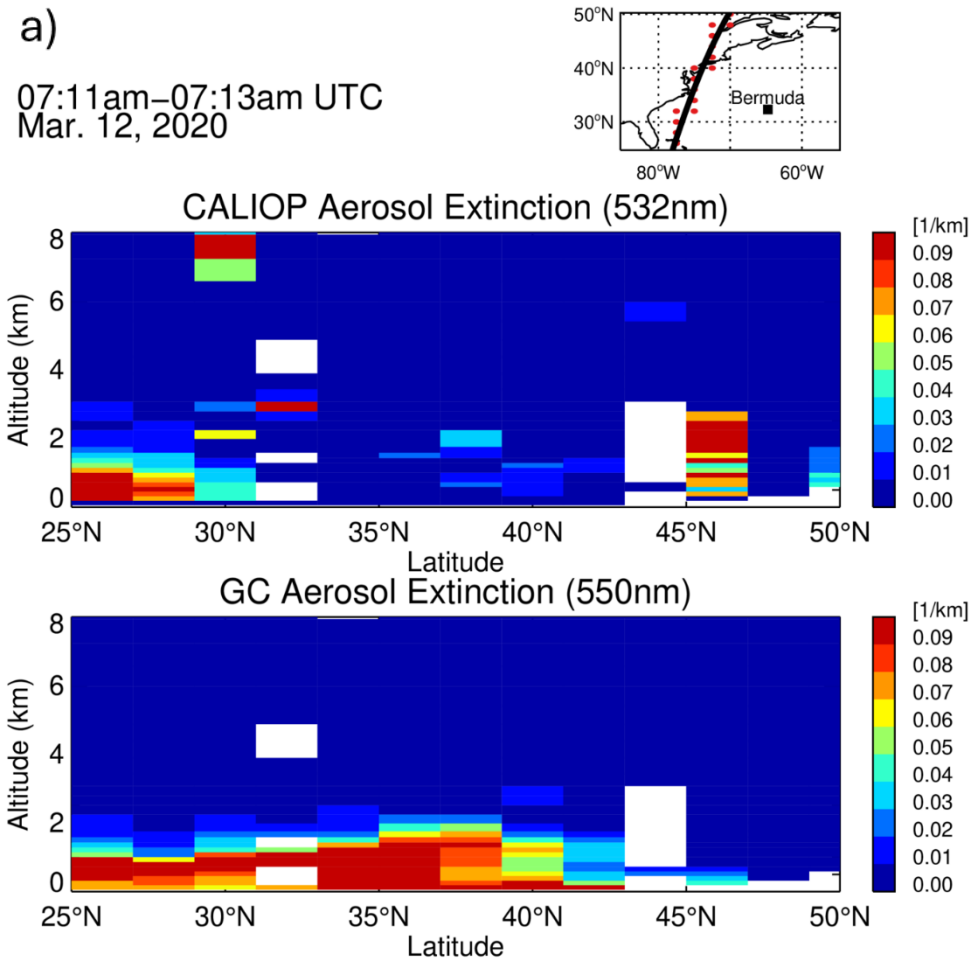

Figure S7. (a) Latitude-height cross-section of aerosol extinctions measured by CALIOP (532 nm) over the WNAO at 07:11-07:13am UTC, Mar. 12, 2020, compared to that of model aerosol extinctions (550 nm). Model output is sampled at ~1:30am LT. **(b)** Left column: Latitude-height cross-section of model speciated aerosol extinctions (550 nm) along the CALIPSO orbit track shown in (a). Right column: same as left column, but for accumulated sea salt (SSa), coarse-mode sea salt (SSc), MERRA-2 RH(%), MERRA-2 cloud fraction, and MERRA-2 effective cloud extinction (i.e., cloud extinction multiplied by cloud fraction to the power of 3/2; Liu et al., 2009). (to be cont'd)

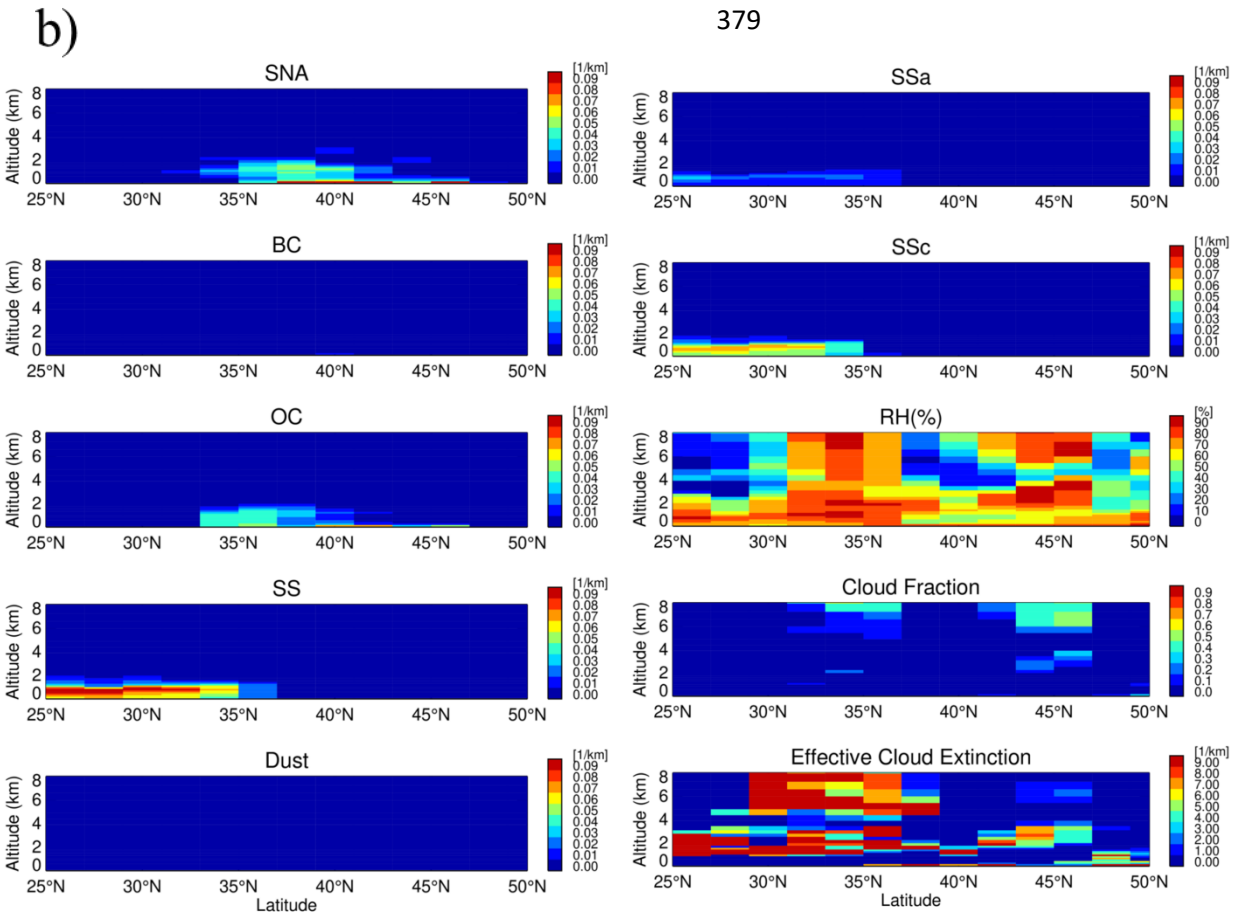

Figure S7. (cont'd)

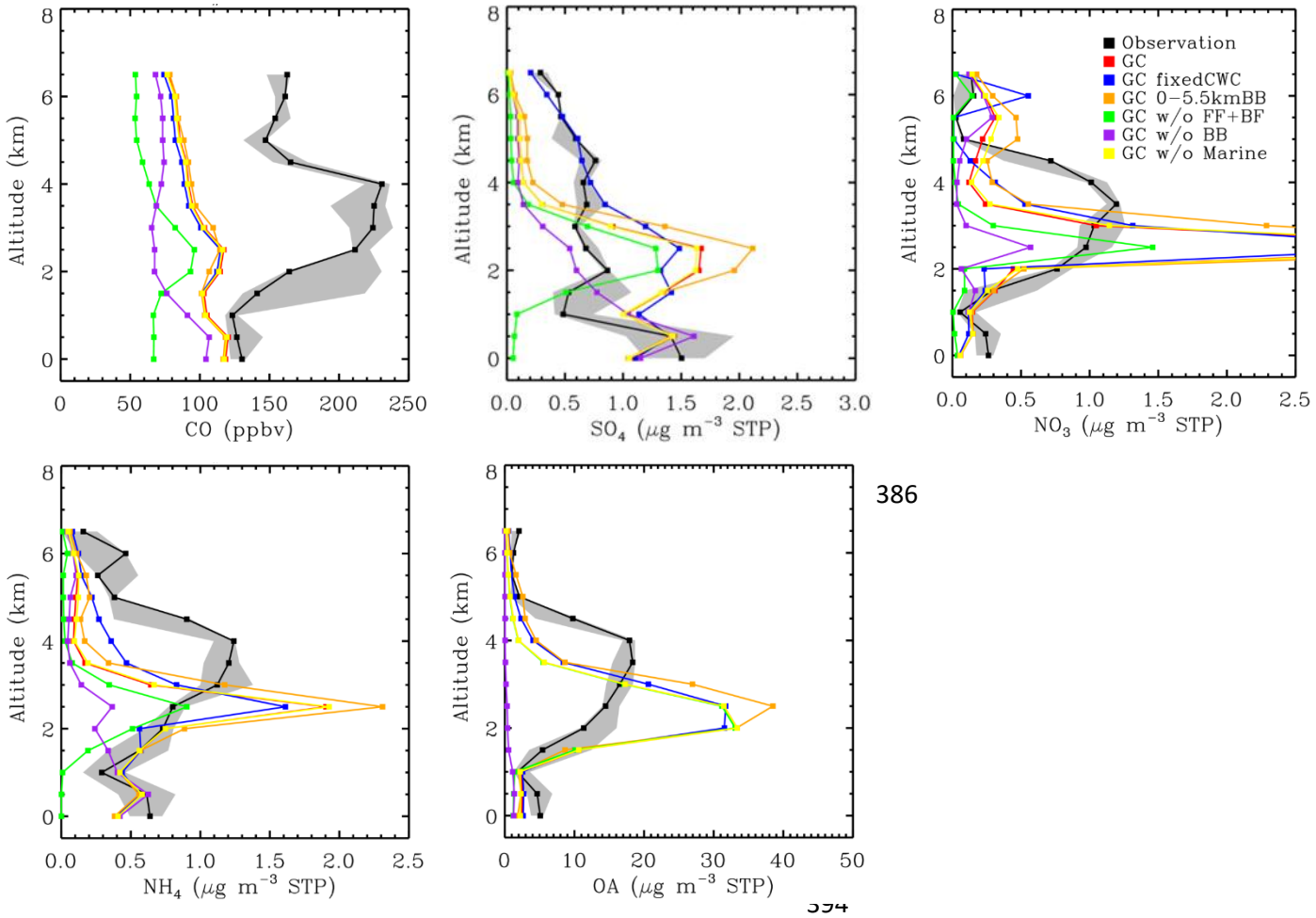

Figure S8. Comparison of model simulated (red) vertical profiles of CO (ppbv), sulfate, nitrate, ammonium, and organic aerosol (OA; μg m^{-3} STP) mixing ratios with Falcon aircraft measurements (black) on Sep. 23, 2020. Also shown are model results from simulations (**Table 1**) with (1) a fixed value for cloud water content used in aerosol scavenging ("fixedCWC"), (2) biomass burning emissions injected to the 0-5.5km altitudes, (3) fossil fuel and biofuel emissions turned off, (4) biomass burning emissions turned off, or (5) marine emissions turned off, respectively. An OA/OC ratio of 2.1 (Philip et al., 2014) is used to convert simulated OC to compare with AMS OA measurements. Hourly model output was sampled at the time and location of aircraft measurements. Values (500m-binned) are medians. Gray shaded areas indicate the ranges of 25^{th} – 75^{th} percentiles for the observations.